

A Simple Method to Test for Energy-Dependent Dispersion in High Energy Light-Curves of Astrophysical Sources

Ulisses Barres de Almeida^{a,1}, M. K. Daniel^{a,*}

^a*Department of Physics, University of Durham, South Road, Durham, DH1 3LE, England*

Abstract

In this paper we discuss a simple method of testing for the presence of energy-dependent dispersion in high energy data-sets. It uses the minimisation of the Kolmogorov distance between the cumulative distribution of two probability functions as the statistical metric to estimate the magnitude of any spectral dispersion within transient features in a light-curve and we also show that it performs well in the presence of modest energy resolutions ($\sim 20\%$) typical of gamma-ray observations. After presenting the method in detail we apply it to a parameterised simulated lightcurve based on the extreme VHE gamma-ray flare of PKS 2155-304 observed with H.E.S.S. in 2006, in order to illustrate its potential through the concrete example of setting constraints on quantum-gravity induced Lorentz invariance violation (LIV) effects. We obtain comparable limits to those of the most advanced techniques used in LIV searches applied to similar datasets, but the present method has the advantage of being particularly straightforward to use. Whilst the development of the method was motivated by LIV searches, it is also applicable to other astrophysical situations where energy-dependent dispersion is expected, such as spectral lags from the acceleration and cooling of particles in relativistic outflows.

Keywords: Time series analysis, gamma-ray astronomy, quantum gravity, particle acceleration
PACS: 95.75.Wx, 95.85.Nv, 04.60.Bc, 96.50.Pw

1. Introduction

The timing properties of a sequence of events can be very revealing as to the physical nature either of the emitting source or of the medium they propagate through, especially when taken in conjunction with information about their energy. Timing analysis algorithms with the capacity of resolving energy-dependent properties can then be an important tool for probing the physical mechanisms leading to flux variability, such as particle acceleration and cooling. Methods are traditionally based on cross-correlation of the binned time-series (e.g. [1]), and sometimes rely on a particular parameterisation of the light-curve, for example by modeling the data according to a pre-determined choice for the light-curve profile (e.g. [2]). In the case of gamma-ray sources, where high-energy processes are responsible for extreme and short-lived variability events, and

*+44 191 334 3678

Email addresses: ulisses@mppmu.mpg.de (Ulisses Barres de Almeida), michael.daniel@durham.ac.uk (M. K. Daniel)

¹Now at Max-Planck-Institut für Physik, D-80805, München, Deutschland.

for which the observational data are often limited by low photon statistics, unbinned methods are the natural and preferential choice of approach to the problem of temporal analysis of time- and energy-stamped photon lists.

In this paper we present a method to search for energy-dependent dispersion in light-curves of transient sources with relatively sparse events, particularly suited for (though of course not limited to) ground-based gamma-ray telescopes. A particular motivation for the study of energy dependent dispersion in the very-high energy (VHE) regime is the prospect of testing for possible signatures of Lorentz invariance violation (LIV), foreseen by a number of theories of quantum gravity (QG) [3]. The analysis method is described in section 2 and its suitability for the particularly challenging task of searching for LIV effects are illustrated in section 3 and applied to AGN lightcurves in section 4.

1.1. Lorentz invariance violation

The unification of the theories of quantum mechanics, governing the smallest of scales, and that of gravity, governing the largest of scales, is one of the most serious challenges in modern physics. Because of the extremely high energies at which QG effects are expected to manifest (around the Planck scale, $E_{\text{QG}} \approx E_{\text{P}} \approx 10^{19}$ GeV) the effects are only likely to become noticeable at very high energies and so difficult to be assessed directly in the laboratory. The so-called time-of-flight experiments, first proposed in a seminal paper by Amelino-Camelia et al. (1998) [4], is one of the most promising ways of carrying out tests for QG signatures. The method is based on the search for an energy-dependent speed of light (c) in vacuum² from the observation of GeV-TeV photons propagating over cosmological distances. The exact form of the energy-dependent photon momentum due to QG effects can vary depending on the particular theory adopted, but given that its effect is very small it can be treated perturbatively leading to a form (eg, following the scheme of [1, 2, 5, 6])

$$c^2 p^2 = E_\gamma^2 [1 + \xi_1 E_\gamma / E_{\text{QG}} + \xi_2 (E_\gamma^2 / E_{\text{QG}}^2) + \dots] \quad (1)$$

The consequently small magnitude of its signature at astrophysically accessible energy ranges³ mean that these searches require extremely sensitive measurements. In time-of-flight experiments the cumulative temporal effects of small variations in c is amplified, eventually manifesting as measurable time-delays over the integrated distance travelled by the photons.

To first order, the magnitude of the time delays expected from QG variations of c are $\delta t \propto E_\gamma / E_{\text{QG}} \sim 10$ s/TeV/Gpc for Planck scale QG. This implies that searches from distant sources are preferred (which in turn can lead to them being correspondingly fainter than nearby sources) and that the searches should be conducted over narrow features (see section 3.2 for further details). For instance, in the case of the active galactic nucleus PKS 2155-304 located at a redshift $z \sim 0.116$, for which we would expect a delay of $\delta t \sim 4$ s per TeV in photon energy, we would need flare features on timescales of no more than tens to hundreds of seconds in the VHE light-curve to bring the effect to the fore. With event rates of a few Hz during the brightest flares [7] the latter property disfavours binning methods on count-rate limited datasets. Sensitivity to small spectral dispersions within very limited photon lists is therefore the most desired characteristic of a dispersion-search method used for time-of-flight measurements.

²This is because in QG theories the vacuum is expected to have a non-trivial refractive index due to fluctuations of the space-time at the quantum level.

³The most energetic photons recorded from astrophysical sources have energies of \sim tens of TeV and for $E_\gamma \sim 1$ TeV the correction to the speed of light due to quantum gravity would be of order $10^{-15}c$

2. Unbinned Methods - Dispersion Cancellation Algorithm

Unbinned algorithms are well-suited for the identification and analysis of local and aperiodic light-curve features, such as bursts or flares in AGN or GRB data. Indeed, the observation of GeV photons from GRB 080916C and GRB 090510 by the Fermi/LAT collaboration [8, 6] has recently been able to set limits at and just above the Planck scale for linear-term effects using two different unbinned approaches. The first of these methods was to directly compare the arrival time of the highest energy photon to the different burst features and, assuming they were contemporaneous at the source, determine what magnitude of dispersion would have to be experienced by the photons during propagation to the observer to explain the observed lag. There are two main drawbacks in such an approach. The first caveat comes from uncertainty in the knowledge of the intrinsic structure of the light-curve, due for example to a lack of understanding of precursor activity in GRBs (see, e.g. [9]), which can cast doubt as to which particular features to associate with the highest energy photons upon assigning the delay. The second drawback has to do with the application of the method to ground-based TeV gamma-ray observations. The poorer energy resolution⁴ of the ground based instruments ($|\Delta E|/E \sim 15 - 20\%$) in comparison to the Fermi/LAT resolution (generally $|\Delta E|/E \lesssim 10\%$ above 1 GeV [10]) would mean that the uncertainty in the dispersion of a single photon (of a few s/TeV) could easily hide any anticipated dispersion.

A number of different approaches exist that are specifically designed for tests of time lags between event sequences, such as likelihood methods [11] and modified cross-correlation functions applied to the individual photon events [12]. A particularly attractive and simple algorithm was the second approach used in the Fermi analysis of GRB 090510. This method was conceived to solve the problem of detecting energy-dependent time lags in statistically limited photon lists, and the fundamental idea of such a *dispersion cancellation* algorithm⁵ method was independently proposed by Scargle et al. (2008) [13] and Ellis et al. (2008) [14] – the latter derived actually to search for QG signatures from neutrino propagation. We also use this technique as the basis for our search methodology, but introduce a different test metric that is better suited to the systematic uncertainties associated with a VHE photon dataset, in particular the poorer energy resolution.

In general, if the expected energy-dispersion is small compared to other relevant variability timescales of the astrophysical system under study, its exact functional form is of little importance, since the dependency can be treated perturbatively and expressed as the first-order terms of a Taylor series (cf. equation 1). The *dispersion cancellation* algorithm uses this fact and works directly on the time- and energy-tagged events to search for a non-zero parameter τ (measured here in s/TeV) that optimally cancels any spectral dispersion present in the light-curve. The lag-correction, δt_i , on photon i of energy E_i , is given by:

$$\delta t_i = -\tau E_i^\alpha \quad (2)$$

where α defines the dominant term of the series expansion for the energy dependency of the time lag, usually taken to be the linear expansion term $\alpha = 1$, or the quadratic term $\alpha = 2$. The *dispersion cancellation* algorithm cycles through a range of possible values for τ , looking for

⁴The energy resolution is defined as $|\Delta E|/E$, where ΔE is the difference between the true energy and the analysis-reconstructed energy of an event.

⁵This name was coined by Scargle et al. (2008) in the context of their particular version of the test, but we will adopt it here with greater generality

the τ^* that extremises an appropriate metric (or “cost function”), chosen to quantify the presence of spectral lags. An advantage of this approach is that it makes no *a priori* assumptions on the nature of the lightcurve apart from the inevitable hypothesis of simultaneity of emission at the source.

A number of different test metrics have been proposed for the purpose of quantifying the spectral lag and finding the optimal dispersion cancellation parameter. They all use some kind of measure of sharpness of the peak in the burst profile as the value to be maximised in the search for τ^* (see examples in [14], [5] and [13]). Here by “sharpness” of a burst we mean a quantity proportional to the gradient of the photon density at the time of the maximum in emission. The principle behind the maximum sharpness choice is that whilst the emission of high and low energy photons at the source is simultaneous (top left panel of figure 1), an energy-dependent dispersion introduced during the photon propagation will always skew the overall light-curve. In the particular example shown in figure 1, this happens by the delayed arrival of the higher energy photons (lower left hand plot), thus skewing and broadening the burst profile as a result. The maximally sharp burst configuration will be retrieved when the temporal sequence of events is again randomised in energy, corresponding to the exact cancellation of the dispersion. Observe that this approach will always give a unique solution for each given dispersion model, because in the case of under- or over-corrections, τ , the asymmetric effect will either still be left present or be re-introduced in the opposite direction, and the burst will remain broadened in respect to its original width. The cost functions used in [13, 6] serve well to minimise the total inter-photon spacing within the entire event sequence, thereby maximising the peak of the lightcurve, but the poorer energy resolution of the ground-based instruments limits the efficacy of the method when applied to VHE observations of sharp bursts. In this paper we examine an alternative test metric based on the Kolmogorov distance between two probability distributions, which better exploits the fact that, whilst the energy resolution of an individual photon is far from ideal, the overall energy bias of a sample of them is actually $\sum_i \Delta E_i \simeq 0$.

2.1. The Minimum Kolmogorov Distance Metric

For a data-set with a sufficient number of photons (a few tens), the event list can be separated into low- and high-energy bands, forming two independent datasets. In the absence of any spectral dispersion, the basic assumption that the temporal sequence of events is randomised in energy should hold and the profiles (apart from statistical fluctuations plus some arbitrary intensity scaling that can be eliminated by normalisation) should superpose. If, however, a systematic spectral dispersion is present, the profiles of the light-curve will look skewed relative to each other (see Figure 1, lower panels).

Given two random variables X and Y in \mathbb{R} , a simple measure of the difference between their respective probability distributions is the *Kolmogorov distance* D_K , defined as the maximum vertical distance between the two cumulative distribution functions (CDFs) [15]:

$$D_K \equiv \sup_{x \in \mathbb{R}} |F_X(x) - F_Y(x)| \quad (3)$$

where $F_X(x) = \text{prob}(X \leq x)$ and $F_Y(x) = \text{prob}(Y \leq x)$.

The situation is illustrated in the right-hand plots of figure 1. Assuming that the events are generated simultaneously and co-spatially in the source, any energy-dependent dispersion introduced between the two will show up as an increased D_k between the cumulative distribution functions of their arrival times. Therefore, minimising this value will amount to cancelling any dispersion present (simultaneously minimising the sharpness of the profile). It is well known

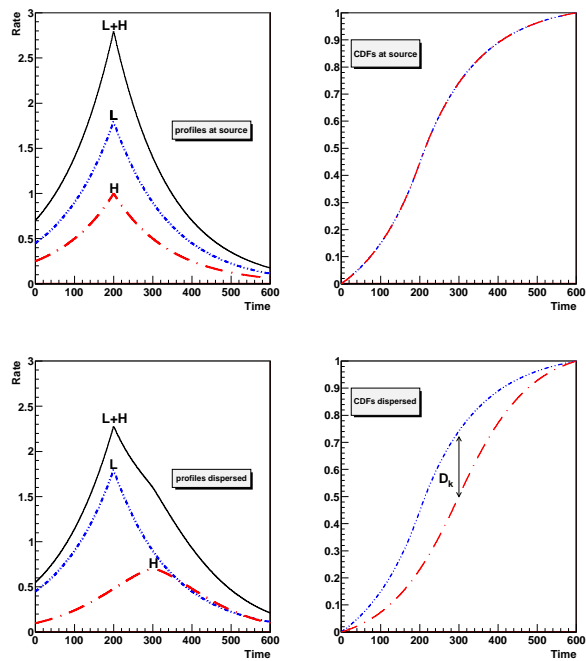


Figure 1: Cartoon of the effect of the energy dependent dispersion on the shape of the low (L) and high (H) energy profiles. Observe that the systematic shift on the high-energy curve relative to the low-energy one induces a skew to the burst. The panels to the right show the corresponding discrepancy in the cumulative distribution function. The maximum vertical distance is indicated, corresponding to the Kolmogorov measure D_K . Observe that D_K tends to fall always in the middle of the distribution, near the peak position of the profiles.

from the properties of the Kolmogorov-Smirnov test that the Kolmogorov distance is insensitive to the tails of the distributions, where the CDFs converge to the values of 0 and 1, and which describe the probability of extreme events [16]. In fact, D_K will tend to fall around the central regions of the CDF, near to the peaks of the profiles where their accumulated discrepancy is maximum. This is a useful property because it means that the measure naturally attributes a greater weight to the most transient parts of the light-curve, whilst being relatively insensitive to outliers.

3. Performance of the Method

We now analyse the performance of the method by discussing the four main factors that are expected to affect the sensitivity to detect energy-dependent dispersion: burst width (section 3.2), energy resolution (section 3.3), burst intensity and asymmetry (section 3.4). Before we move on to discussing these specific topics, we list the steps for application of the algorithm:

- select a burst or transient event from the light-curve;
- split the burst photons into low- and high-energy datasets, this will be a trade-off such that both groups have the largest possible number of events in them, but also that the difference between their average energy is as large as possible;
- build the CDFs for the two distributions (see Appendix A for some discussion on alternatives ways of representing the lightcurve);
- adopt a model for the time delay, e.g. linear or quadratic in energy;
- apply correction to the time-stamp of photons according to equation 2;
- for each value τ of the correction, calculate D_K ;
- the optimum τ^* is the one which minimises D_K for the range of τ tested;
- assess the uncertainty by simulation of the burst or bootstrap of the data.

For illustrative purposes, we will only consider in this section the ideal case of an isolated Gaussian burst. The superposition of multiple bursts or burst shapes different from Gaussian will be discussed when the method is applied to real flare data from the AGN PKS 2155-304 in the next section, but do not change the conclusions presented here. For our studies individual burst data were simulated using the generalised Gaussian shape [17], which can also provide a good match to the pulse profiles generally observed from AGNs and GRBs:

$$I(t) = I_{max} \exp \left[- \left(\frac{|t - t_{max}|}{\sigma_{r,d}} \right)^\kappa \right] \quad (4)$$

where t is the time into the flare, t_{max} is the time of maximum flux I_{max} , σ_r and σ_d are the signal rise (for $t < t_{max}$) and decay (for $t > t_{max}$) time constants respectively, the ‘‘sharpness’’ (peakedness, or kurtosis) of the profile is given by the parameter $\kappa > 0$. A low value of κ means a sharply peaked pulse, a high value a more rounded one, and $\kappa = 2$ corresponds to a Gaussian pulse shape. The rise (t_r) and decay (t_d) times from half to maximum amplitude are found from the rise and decay constants using the equation $t_{r,d} = [\ln(2)^{1/\kappa}] \sigma_{r,d}$. The spectra are assumed to take a power law shape of the form $dN/dE = kE^\Gamma$, where Γ is the spectral index and k a flux constant.

3.1. Energy cuts

The first step necessary in constructing the CDFs for the analysis means we must decide where to place the low- and high-energy boundaries. This choice is made such that the difference in the mean energy between the two CDFs can be maximised, while keeping good photon statistics in both energy bins for the analysis. We have verified that due to the (usually) steeply-falling spectral index of the photon distributions, the analysis is less sensitive to the choice of the low-energy boundary, provided this is set comfortably above the threshold energy of the instrument. We set here the low energy band to be $0.2 \leq S \leq 0.4$ TeV. We then searched for an optimal high-energy cut window, which will be the more statistically-starved component. Simulations were for a Gaussian light curve shape of 120s rise/fall time and a maximum count rate of 3 Hz.

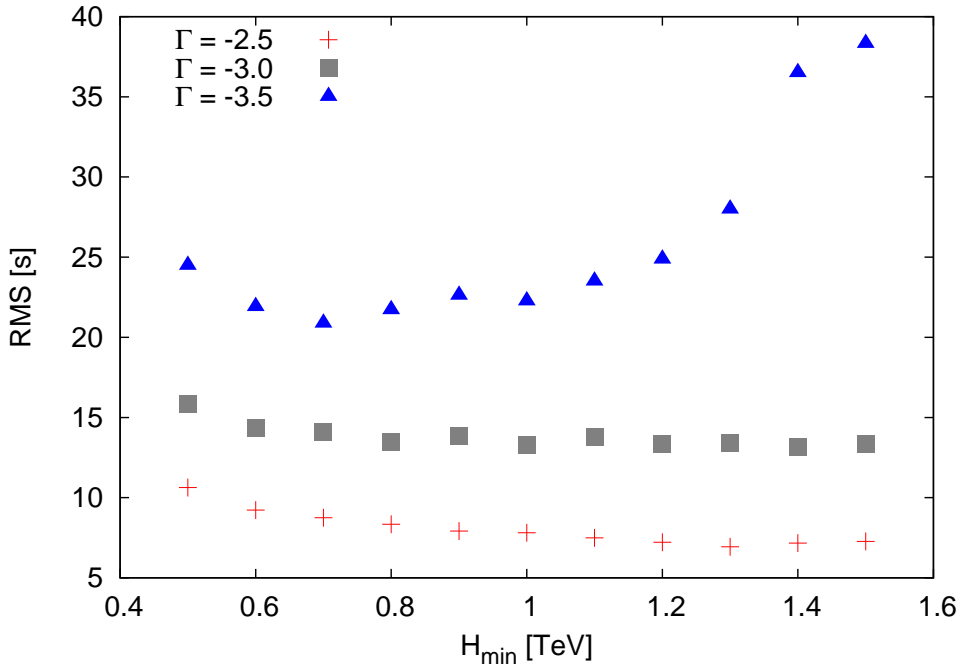


Figure 2: Effect of the choice of the minimum energy cut for the high energy band (H_{\min}) on the accuracy of the determined dispersion measure. Simulations are for power law spectra with indices of -2.5 (crosses), -3.0 (squares) and -3.5 (triangles).

Figure 2 shows the results of our analysis on the effect of the choice of the minimum value for the high energy cut H_{\min} on the root-mean-square (RMS)⁶ of the reconstructed dispersion parameter (τ^*) for three different values of the spectral index (for $\Gamma = -2.5, -3.0, -3.5$). The curves for each spectrum show a slight improvement of the RMS with increasing energy cut which quickly plateaus. This is because at too low a minimum energy for the high energy sample

⁶The root mean square of a distribution X with N events x_i is given by $RMS = \sqrt{\sum x_i^2/N}$.

the difference in the average photon energy of the events gets too low and the high-energy CDF becomes indistinguishable from the low energy CDF as they are both dominated by events that are not dispersed much. The error in any reconstructed lag correspondingly increases as natural statistical fluctuations become the dominant source of uncertainty. Much more noticeable for this though, is the steep rise in the RMS for $H_{\min} > 1$ TeV for the softest energy spectrum ($\Gamma = -3.5$). This occurs when the number of events in the high energy sample drops below ~ 10 – the CDF becomes ill-defined with respect to the low energy sample CDF and so no reliable dispersion measure can be found. This result gives an idea of the minimum number of events necessary in an energy band for the method to be able to work. From this we see that the results of the test will be fairly independent of the actual minimum high energy cut, provided the high energy band has > 10 events and is at least a factor of two higher in energy than the lower energy sample. We take $H_{\min} > 1$ TeV for the remainder of the paper, unless specified otherwise.

3.2. Sensitivity to burst width

We quantify the sensitivity to the burst width by the term “sensitivity factor”, η , following the definition in [4]. This quantity is written as the ratio of the expected dispersion magnitude (δt) to the width of the transient feature (Δt):

$$\eta = \frac{\delta t}{\Delta t} \quad (5)$$

This ratio is the main parameter which will quantify the size of the lag that can be probed by the method, for a given burst width.

For this analysis, we simulated 10,000 Gaussian burst profiles of 500 events each, with a low-energy threshold of 200 GeV and a spectral index $\Gamma = -2.5$. A dispersion was then introduced that varies from 5-200% of the burst width, i.e. from the dispersion being entirely contained within the burst to the burst being smeared in time over a period greater than its duration. The results are shown in figure 3, where the points correspond to the mean reconstructed τ^* and the error bars are the RMS of that distribution. We see, as expected, that the narrower the width of the burst with respect to the introduced delay, the better the delay can be determined. The error bars in the plot indicate the 68% confidence intervals (CI) of the reconstructed lag distribution, showing that the method can reconstruct the correct value of τ and exclude the null hypothesis of zero lag at the 99% level up to a value of $\eta \approx 0.2$. This corresponds to a sensitivity limit of a lag equal to 20% of the burst width.

3.3. Sensitivity to energy resolution

We also included in our sensitivity analysis the effect of the energy resolution ($|\Delta E|/E$), an important consideration in ground-based gamma-ray measurements. This uncertainty will directly affect the dispersion correction for individual photons and will thus limit the sensitivity of the method. The energy resolution is modelled as 0% (an ideal detector case where the reconstructed energy is always the true energy), 10% and 20%, shown as the sub-sets of data in figure 3. There is a small systematic trend for the reconstructed lag to be under-estimated as the energy resolution gets poorer, but this is very small in comparison to the overall error in the reconstructed τ^* . The under-estimation is expected: the power law nature of the spectrum means that any width to the energy resolution will systematically spill more photons to higher reconstructed energies than photons to lower reconstructed energies by sheer weight of numbers. This is a well known problem in spectral reconstruction of VHE sources. It is possible, with appropriate Monte Carlo modelling or bootstrapping, to compensate for this systematic trend if necessary.

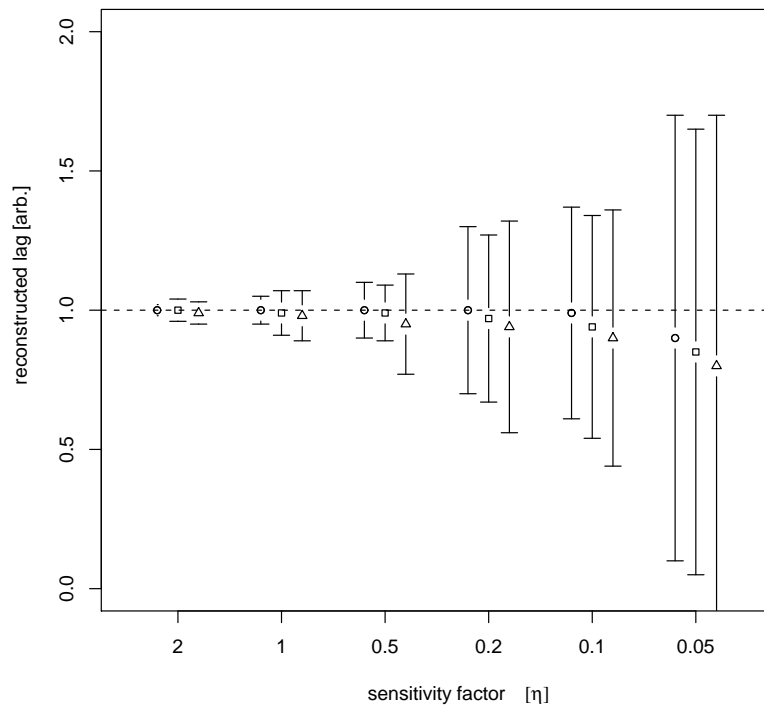


Figure 3: Sensitivity of the algorithm to the ratio lag/burst width η for 0% (open circle), 10% (open square), and 20% (open triangle) energy resolution. The results are from sets of 10,000 Monte Carlo simulations of Gaussian profiles, containing 500 events each, for a low-energy threshold of 0.2 TeV and spectral index $\Gamma = -2.5$. The low- and high-energy bins were defined such that the average energy difference between the two is ~ 1 TeV.

3.4. Sensitivity to burst intensity and asymmetry

The burst intensity is another factor that will affect the sensitivity of the algorithm, since it will limit the photon statistics available to construct the CDFs. This is shown in figure 4 and was tested over a similarly-generated set of Gaussian profiles as before. Here bursts were generated with differing numbers of events, between 50-3000, accounting for different count rates (corresponding to I_{max} between 1-10Hz) and for 3 different burst widths, with rise/decay times varying between 10-120s.

For a given burst width, the effect of increasing the number of events in the light curve is to reduce the RMS of the recovered dispersion parameter. From a certain number of events onwards, and depending on the width of the burst, the distribution tends toward a plateau and little improvement in the RMS is obtained by further increasing the number of events. As noted earlier, the sharper the burst, the earlier this plateau is reached. Finally, we have also tested for any effects due to profile asymmetry by maintaining the total burst width and varying the ratio of rise/decay time of the flare. The results plotted in Figure 4 show that the method is not affected by any intrinsic burst asymmetry, but only by its overall width.

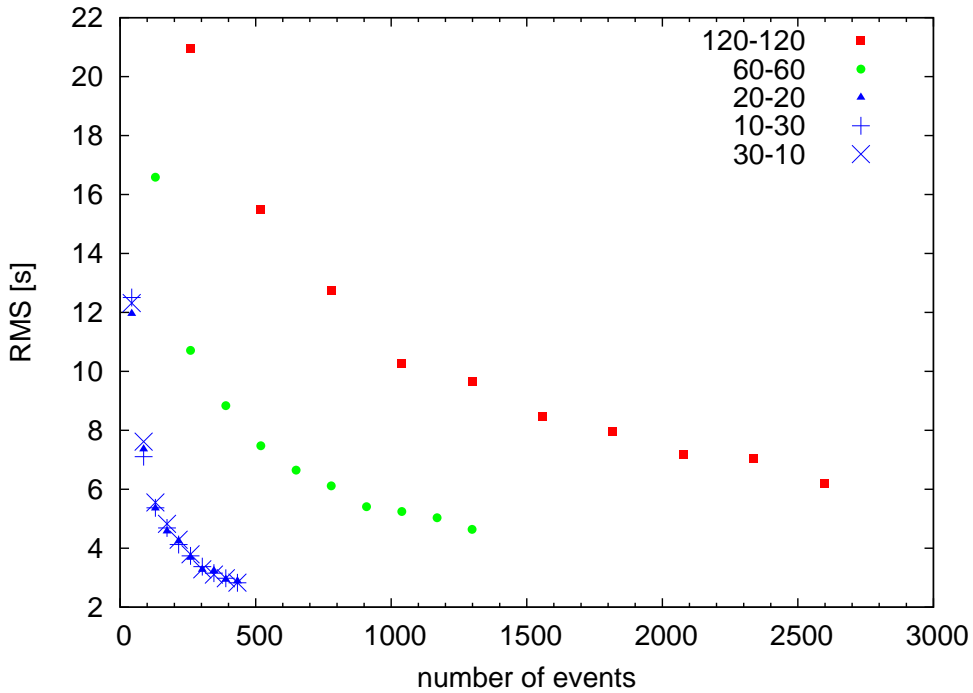


Figure 4: Sensitivity of the method in relation to the width of the burst and the number of events in it. The labels in the key define respectively the rise and fall times of the profile. The results are from MC simulations of 10,000 bursts with a maximum count rate between 1-10Hz.

3.5. Sensitivity to energy spectrum

The observation of a single burst or flare is not going to provide definitive evidence (or refutation) of energy dependent dispersion due to QG. Instead, a number of sources demonstrating

a consistent behaviour for a range of redshifts will be necessary to be able to confidently determine if such an important effect exists, and to disentangle it from source-intrinsic lags. Even if the intrinsic spectrum for a given source type is identical between objects, the interaction of the gamma-rays on the diffuse extra-galactic background radiation will lead to a softening of the observed spectral index with increasing redshift. The number of very high energy events is intimately related to the energy spectrum; to quantify the systematic uncertainty introduced by this effect in the estimate of τ^* , we simulated 10,000 Gaussian shaped lightcurves, with 120 s rise and fall times and a maximum count rate of 3Hz, for a range of indices Γ between -2.5 and -3.5. The RMS of the recovered τ^* is plotted in figure 5, demonstrating an approximately linear deterioration on the determination of τ^* as the spectrum softens. This effect is also easy to understand as the softening of the spectrum represents a depletion of high-energy photons from the high-energy CDF.

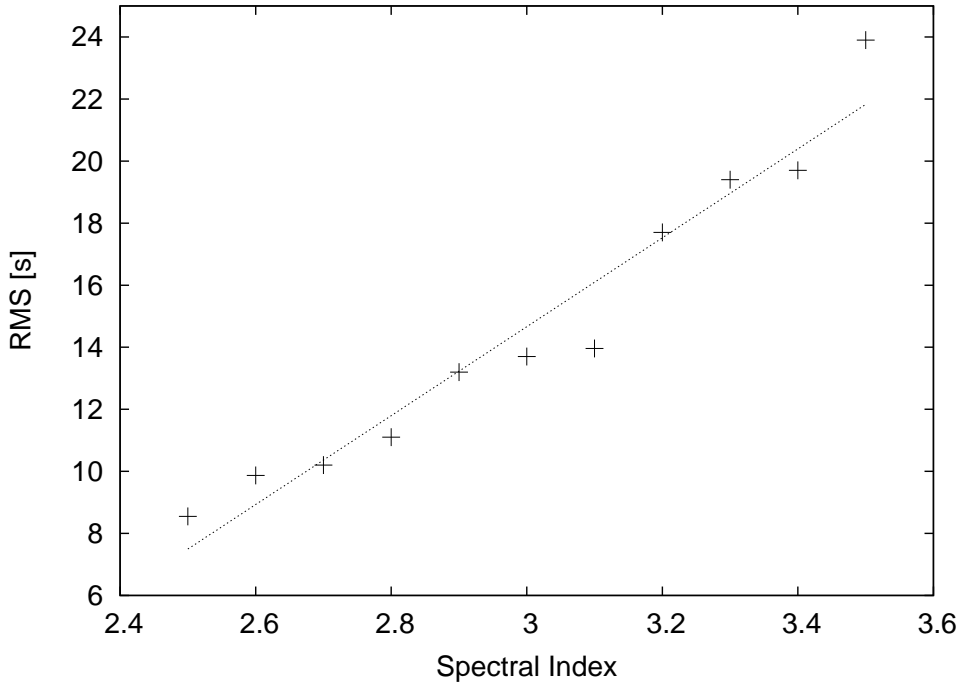


Figure 5: The effect of the spectral index on the uncertainty in the recovered dispersion. The simulated bursts have a width of 120 s, meaning that the recovered dispersion's RMS varies from 0.5-20% of the burst width, for an index Γ going from -2.5 to -3.5.

3.6. Burst analysis window

Until now we have treated simulated isolated bursts, for which we are confident it is straightforward to find a reasonable signal-to-noise ratio above background from which we can define the burst to start/end. When analysing transient events within a real light-curve, as will be done

in the next section, it is important to consider the effects of confusion and under-sampling of individual bursts. If the burst is adjacent to other structures within a complex lightcurve it might be difficult to define with precision its start and end times, and a superposition of different features might be unavoidable. In particular, the highest energy, most-lagged events could then fall outside an inappropriately chosen analysis window, thus affecting the profile reconstruction. Also, if the burst is at the edge of an observation run, data could be missing for part of the flare, this loss of information will also be energy-dependent if there are lags in the light-curve and this is likely to affect the performance of the reconstruction.

To test for these effects and assess if a proper reconstruction of the original profiles of lagged light-curves is still possible within our framework, we performed two sets of MC simulations, for which we generated two groups of 10,000 Gaussian bursts with 500 events each, a spectral index of $\Gamma = -2.5$ and an energy resolution of 20% was used.

For the first set, represented in figure 6, the analysis considered a series of windows around the peak position of the burst of widths equal to 1, 2, 3 and 5 times the combined rise/fall time ($t_{r,d}$) of the burst (where these relate to the time for full-width-half-maximum $t_r + t_d = t_{FWHM}$), to simulate different degrees of under-sampling. In this case, a so-called “transparent window” was used. This means that the CDFs are built only with the events that fall within the time window boundaries after the dispersion cancellation has been applied, but for each different value of τ events are allowed to pass into and out of the window’s boundaries – updating the CDF at each new step of the algorithm.

The result is that a very narrow window around the burst affects the accuracy of the reconstruction, increasing the RMS by up to 20% when only the FWHM around the burst peak is used to build the CDF. This degrading effect can be understood as a consequence of an ill-defined shape for the CDF. The effect is present for all the range of sensitivity factors tested, being more pronounced for smaller η . This suggests that in using the method one should attempt to include as much of the burst as possible into the analysis, in order to include the most possible information on the profile shape for the CDF comparisons. An arbitrary choice of a narrow window about the peak of the burst to artificially reduce η does not improve the results, due to a loss of information in the CDFs on the shape of the wings of the distribution. Of course this observation is no prescription for the analysis. Ideally the time window around the burst should be at least $3t_{FWHM}$, but in the case that the burst is confused with other features the analyser should simply be aware of this degrading factor when determining the confidence intervals for τ .

This also demonstrates that whilst individual sub-flare features may be resolved, they can still potentially influence each other. If a train of bursts is too closely aligned with respect to each other for an individual analysis to be conducted, then our simulations show that the critical factor is to account for the rise/fall parts of the profile of the first/last burst respectively. In such cases, the best approach to the analysis is to consider the train of bursts together, rather than trying to split the bursts into ill-sampled individual features.

As a final note, in the same way that events pertaining to the burst can be selected out of the analysis window, events not pertaining to the burst can also contaminate the analysis during the cancellation procedure, for instance from background events or from superposing bursts closely aligned in time. This will produce similar kinds of effects as the case treated in figure 6. As before, a compromise has to be found (if necessary via dedicated simulations with a configuration as similar as possible to that of the real lightcurve) between reducing the contamination and sampling well the profile of each individual burst.

There is a second class of situations when a burst will be under-sampled at the detection level rather than in the analysis procedure, for instance when the burst occurs close to the start/end

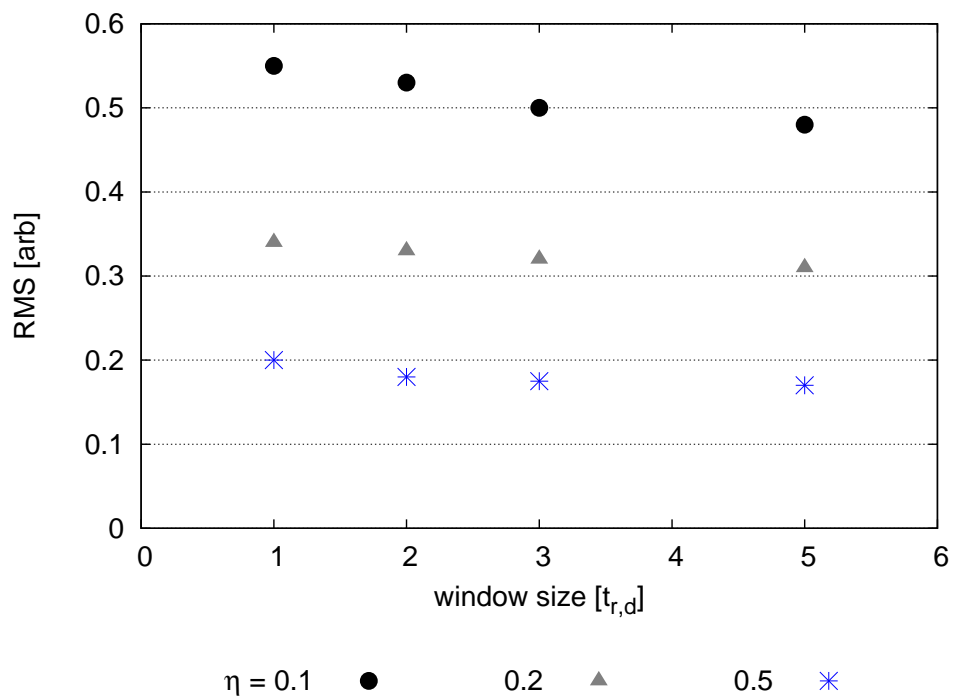


Figure 6: Sensitivity of the Kolmogorov distance method in relation to the size of a “transparent” window used to reconstruct the CDFs from the burst profile. The labels in the key define different data sets with different sensitivity factors $\eta = 0.5$ (star), 0.2 (triangle), 0.1 (circle). The results are from MC simulations of 10,000 bursts generated from a Gaussian shape and an associated energy resolution for each event of $\sim 20\%$.

times of an observation run. In this case, events are lost permanently. To simulate this effect we introduce a so-called “opaque window” in the analysis, where events that are initially out of the analysis window for a $\tau = 0$ will not be admitted in as τ changes during the steps of the cancellation algorithm. The results are shown in Figure 7. In this case, the fact that we *permanently* lose a high proportion of high energy events (because they are more spread or dispersed than the low energy ones) means that not only will the RMS be worsened, we preferentially lose the events that will most accurately recover the correct dispersion.

The three different data groups represented in Figure 7 are for sensitivity factors η equal to 0.5, 0.2 and 0.1. Note that the case of longer duration bursts is the most affected, simply because in this case more high-energy events are permanently lost from the burst window, relative to the low- η case. Within each dataset, points 1-5 indicate the size of the window in units of t_{FWHM} . Here, the permanent loss of information about the most-lagged events mean that the true lag τ^* is reconstructed wrongly the closer the burst maximum is to the start/end of the observation window. Therefore, as before, the conclusion is that windows as wide as $\sim 3t_{FWHM}$ around the flare peak give the best compromise between burst width and information content. Another conclusion from this analysis is that the search for lags in a flare for which a large portion is missing from the burst (more than 1/4 of the total number of events) is certainly not recommended, so observation strategies that maximise the amount of on-source time in lightcurve monitoring (such as [18]) are definitely encouraged.

In any case, as before, a complete simulation, or bootstrap, of the observed light-curve is the best way to assess the correct RMS from the combined effect of all cases discussed in this section. An example of this approach to the analysis of real data-sets is given next.

4. Application to PKS 2155-304 flare simulations

In the previous section we have discussed all the principal factors contributing to the uncertainty in the reconstructed lag. We have illustrated those by the simple case of isolated Gaussian bursts. We are now in a position to test the efficacy of the method to recover a dispersion in some realistic lightcurves. To do so, we move from the simple tests on Gaussian profiles to work on simulated datasets based on fitted profiles for the large flare of PKS 2155-304 from 2006 [7]. For consistency with previous work done on the PKS 2155 data set, and to enable people to reproduce our work, we use exactly the same profile fits presented in the original H.E.S.S. publication, instead of searching for and separating the individual bursts ourselves (step 1 of the analysis procedure). This introduces a binned and parameterised aspect to the method, for that is how the lightcurve features were identified in [7]. To keep the method truly non-parametric and unbinned, an approach such as the Bayesian Blocks [19] algorithm to search for the time window cuts could be applied and is recommended, but it does not change the results we present here as this exceptional flare of PKS2155-304 is well resolved.

There are 5 prominent flaring events (labelled BF1-5) noted for this lightcurve, reproduced in figure 8, and the relevant parameters for the generalised Gaussian fits are reproduced in table 1. The simulated event times are generated by random draws from a distribution described by Equation 4, each flare summed to give the total lightcurve. To each event time, an energy value is then randomly attributed from a power law distribution, with $E_\gamma > 120$ GeV. As there was no evidence for any spectral variability (at the $\Delta\Gamma \geq 0.2$ level [7]) during the night, for simplicity we adopted a simple power law distribution with a spectral index of $\Gamma = -3.5$ in our simulations; changing the model to the broken power-law fit given in [7] makes no difference to the general conclusions discussed here. The error in the energy reconstruction of a single event

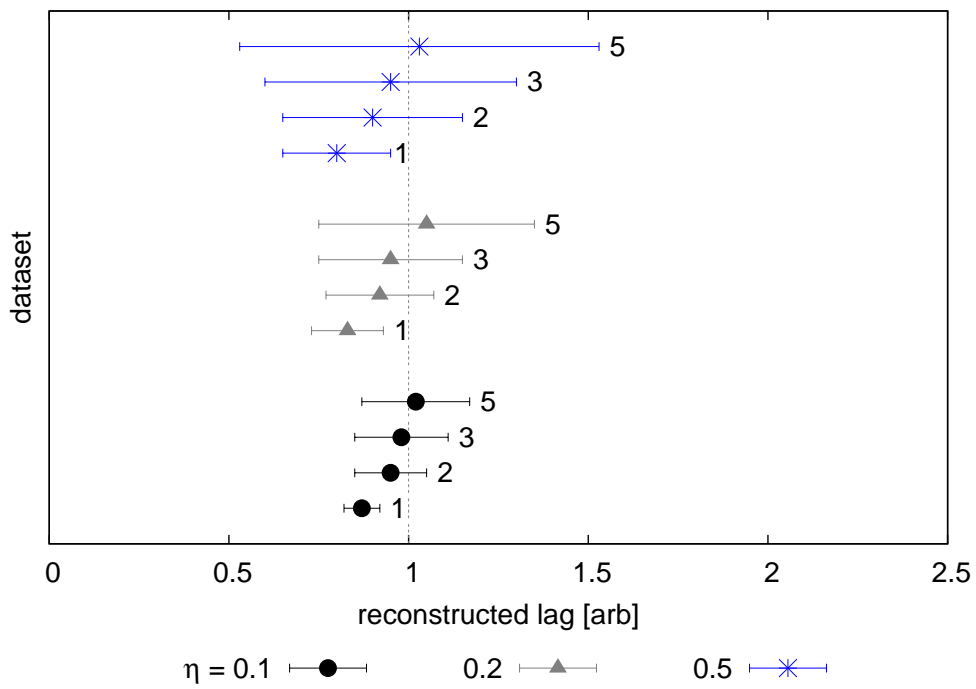


Figure 7: Sensitivity of the Kolmogorov distance method in relation to the size of the “opaque” window used to construct the CDFs from the burst profile. The different datasets correspond to $\eta = 0.1$ (circles), 0.2 (triangles), 0.5 (stars) respectively. The number 1-5 within each dataset are for windows of 1-5 (t_{FWHM}) widths, respectively. The results are from MC simulations of 10,000 bursts generated from a Gaussian shape, and an associated energy resolution to each event of $\sim 20\%$. The actual value of the induced lag is indicated by the dotted vertical line.

is dominated by systematic uncertainties and is estimated to be of the order of 15% throughout the entire energy range. In reality the energy resolution is a function of energy, improving for higher energies, and so this value can be taken as a worst case scenario. Then, to simulate the energy dependent dispersion, a systematic delay τ was applied to each photon's true energy and the recovery procedure was carried out based on the instrumentally smeared energy values.

Flare	t_{max} [s]	Max. Rate [Hz]	σ_r [s]	σ_d [s]	κ
BF1	2460	1.33	173	610	1.07
BF2	3528	1.25	116	178	1.43
BF3	4278	1.99	404	269	1.59
BF4	4770	1.19	178	657	2.01
BF5	5298	0.74	67	620	2.44

Table 1: Parameters used for the generalised Gaussian fit to the PKS 2155-304 flare simulations, based on the original H.E.S.S. analysis results [7]. The third column (Max Rate) refers to the maximum count rate of each burst, corresponding to its peak flux at time t_{max} . The parameters σ_r and σ_d are the rise and decay time constants of each burst and κ a measure of the sharpness of the peak (see text for details).

In a real-case analysis like the one shown here, there are two non-trivial steps (numbers 1 and 2 of the list shown in section 3) that must be considered: (i) the choice of the analysis window around each burst and (ii) the choice of the energy boundaries to construct the CDFs. Figure 9 shows the results of our analysis on the effect of the choice of the high energy cut on the RMS of the reconstructed dispersion parameter for the individual flares. The improvement in the RMS as the cut moves away from the soft energy band is notable. It is followed by the presence of an optimal plateau around and above 1 TeV and worsening RMS above 2 TeV due to a loss of event statistics. All this reproduces what was seen in the ideal flare shape case of section 3.1 and shows the choice of 1 TeV for H_{min} to be a good one. The uncertainty in the reconstructed lags (in s/TeV) were determined from Monte Carlo simulations performed for each individual burst. The top panel of figure 10 shows an example of values of the Kolmogorov distance D_K for each different dispersion parameter τ^* tested in the analysis. The middle panel shows the distribution of D_K versus τ^* for 10,000 realisations of BF2, from which confidence intervals for the lag were derived, as shown in the lower panel histogram.

4.1. Testing the recovery of a known induced dispersion

To demonstrate the efficacy for recovering a dispersion, for each simulated lightcurve in figure 11 we introduced an artificial dispersion between $-100 \leq \tau \leq 100$ s/TeV, which we aimed to recover with the dispersion cancellation algorithm and minimisation of the Kolmogorov metric. The algorithm was applied to each of the five major burst features in the dataset, BF 1-5, generating five sets of independent measurements. Whilst the RMS of the recovered dispersion τ^* leaves uncertainty in the true dispersion τ , the mean of the recovered dispersion is an accurate reflection of the true dispersion. This shows that the measurement of multiple flares from a single object could be used in combination to give a more accurate estimate of any induced dispersion, since they should be the same for all flares if they have an origin in propagation effects. Also, the accuracy of the recovery over a large range of the parameter space demonstrates that a number of objects at different redshifts could then accurately trace a distance dependent (i.e. propagation induced) dispersion.

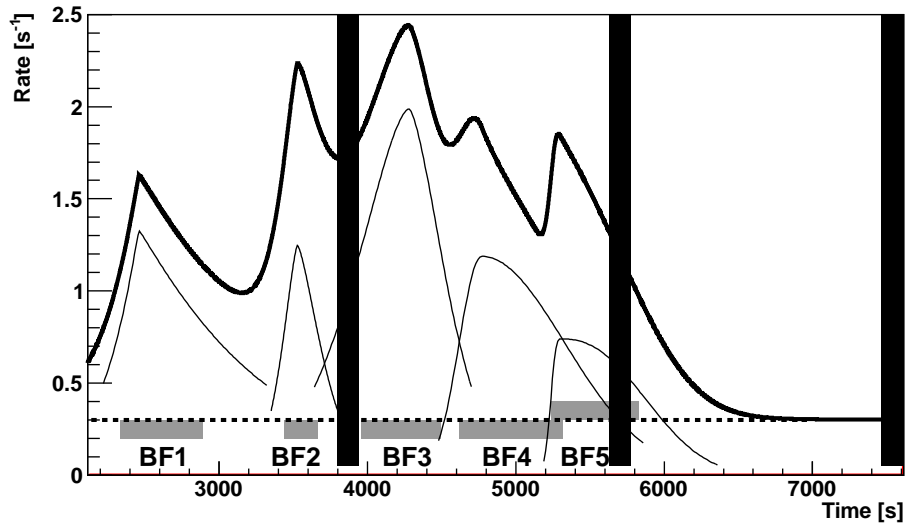


Figure 8: The parent population light curve of the MJD 53944 PKS 2155-304 big flare event simulation. The individual bursts BF1-5 (see table1 are marked by the thin lines and the dashed line shows the constant signal ($\sim 10\%$ of the maximum count rate) onto which the bursts are superimposed. Values are renormalised from the flux values in [7] to count rates here. The heavy line denotes the cumulative light curve. The grey shaded regions mark out the location and extent of the $1-\tau_{rd}$ windows for the bursts, the black bands correspond to the data gaps due to observing run transitions (see section 3.6).

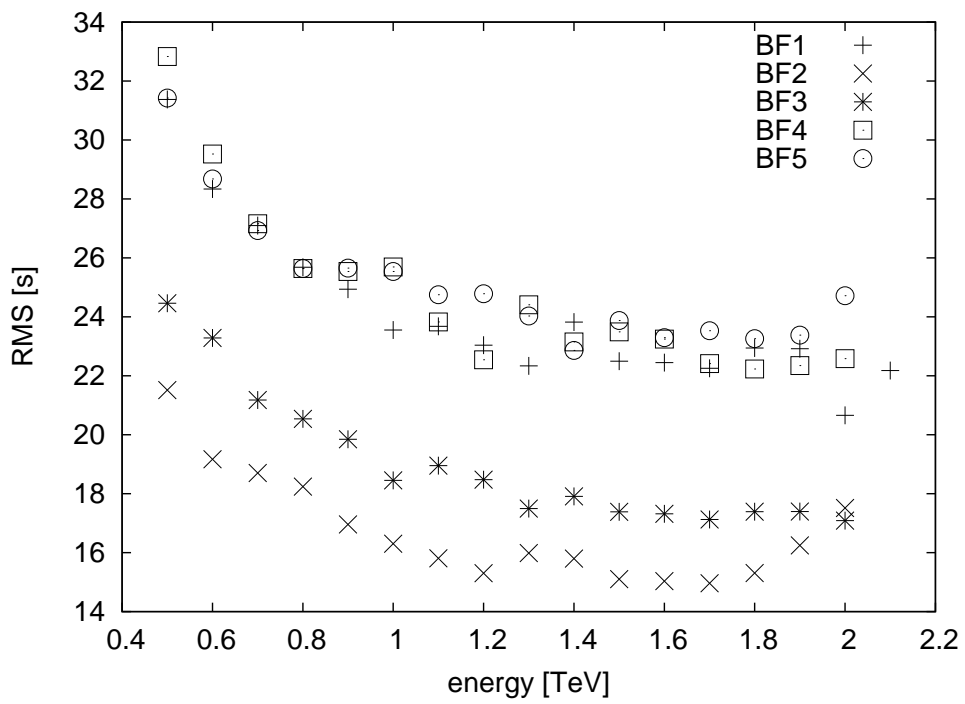


Figure 9: Effect of the choice of the energy cut for the high energy band on the accuracy of the determined dispersion measure based on Monte Carlo simulations of the burst profiles BF1-5 (see text for details).

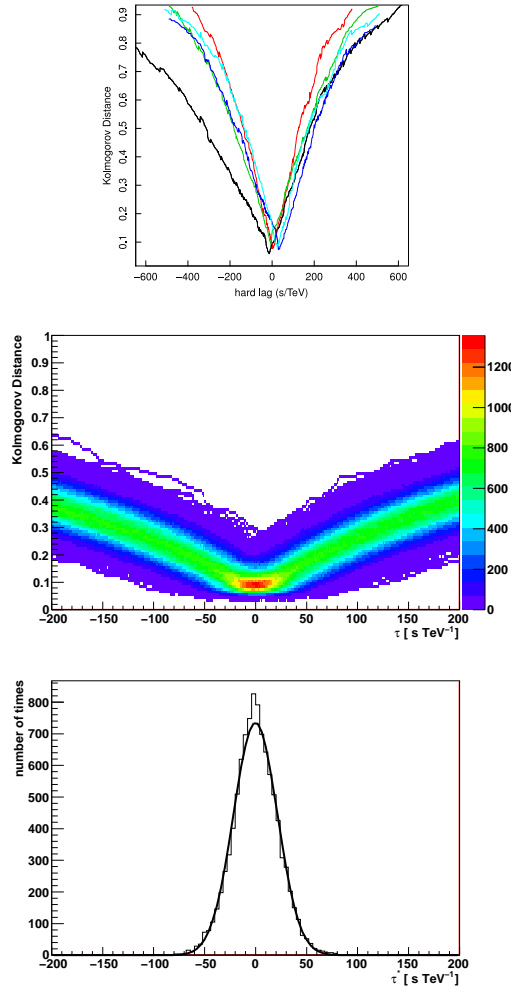


Figure 10: **Top panel:** Kolmogorov distance profiles for different values of τ from the search of energy-dependent dispersion in the bursts BF1-5 of PKS 2155-304. The analyses were performed in steps of 1 s/TeV. **Middle panel:** 2-D histogram of the Kolmogorov distance calculated for each step of τ in 10000 simulated lightcurves for the profile of BF2, with no dispersion introduced. A minimum is always reached with some variance around 0 s/TeV. **Bottom panel:** Histogram of τ^* for each of the minimum D_k values found in the simulations of BF2 shown in the middle panel, centred on 0. The standard deviation of a Gaussian fit to this distribution is used to estimate the limiting accuracy for reconstruction of τ^* .

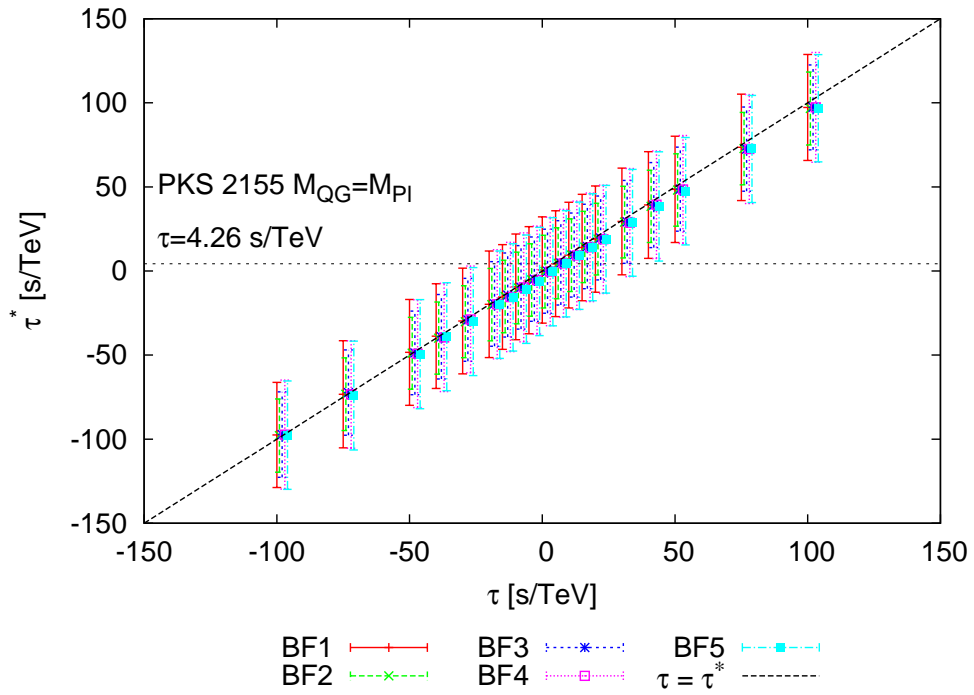


Figure 11: The accuracy to which the method can recover a fixed dispersion parameter introduced into the light-curves representing each of the sub-flares of PKS 2155-304. Each point is the average dispersion estimated from 10,000 simulated lightcurves and the errors represent the RMS of the recovered dispersion parameter, τ^* . Values corresponding to the different flares are slightly offset on the x-axis for visual clarity. The dashed line is a guide to the eye of $y = x$, not a fit to the data. The dot-dashed line represents the expected linear dispersion for a Planck mass scale of quantum gravity from a source at the redshift of PKS 2155-304.

4.2. Estimating the limits to QG measurements from the Kolmogorov metric

It is known from previous studies of this dataset that there is no spectral dispersion present in the PKS 2155-304 big flare night lightcurve that is large enough to be detectable within current instrument’s sensitivities. We therefore limit ourselves to using the simulations of the dataset as a test-bed for assessing the sensitivity of the method in a real-life case. The E_{QG} sensitivity limits that could be placed from the application of the algorithm to the big flares from PKS 2155-304 are presented in table 2. We adopted a linear relation between the lag and energy of the photon ($\alpha = 1$ in equation 2) for the E_{QG} limit estimates in the final column. The mean energy difference $\langle \Delta E \rangle$ between the low- and high-energy profiles is also given. Note that the sensitivity limits obtained here are comparable with the most constraining results achieved to date from more complex analyses of this particular flare [2]. This result shows that this simple method has the potential to probe QG effects to *at least* the same levels achieved by the current tests using AGN, with the advantage that, by separating the light-curve into multiple bursts, from a single dataset we can derive multiple independent measures of the same quantity.

Flare	$\langle \Delta E \rangle$ [TeV]	σ_τ [s/TeV]	E_{QG} [10^{19} GeV]
BF1	1.42	± 24.1	> 0.15
BF2	1.23	± 16.4	> 0.19
BF3	1.40	± 18.6	> 0.2
BF4	1.25	± 24.4	> 0.13
BF5	1.29	± 24.5	> 0.14

Table 2: Results for each of the PKS2155 big flare night sub-flares $\langle \Delta E \rangle$ is the mean energy difference between the low- and high-energy CDF. $\sigma_{\tau_{\text{tau}}}$ corresponds to the standard deviation of a Gaussian fit to the histogram of τ^* from 10,000 simulated lightcurves. The sensitivity limits on E_{QG} correspond to the 95% confidence levels from the uncertainty in the recovered τ^* . Note that these values are not real estimates of E_{QG} limits from the PKS 2155-304 observations, but sensitivity estimates to searches in a simulated dataset.

It is apparent in figure 11 that any dispersion $|\tau| < 50$ s/TeV is unlikely to be confidently determined from an individual flare observed with the current generation of Cherenkov telescopes. The exceptional flares described here each have too small a value of η to resolve such a signature individually, the even longer typical widths of observed VHE AGN flares only serves to reinforce this point. Nevertheless, the fact that lags can be accurately reconstructed over a large range of τ , demonstrated by the correct mean value of the reconstructed lags, supports the idea that the combined results of a number of flares from an individual source could improve the E_{QG} limits considerably for each given object.

5. Discussion and Conclusions

We presented here an unbinned, non-parametric method of testing for energy dependent dispersion in a lightcurve that is sufficiently robust to work under the constraints of scarce counting statistics and the modest energy resolution expected for VHE gamma-ray data analysis, the latter issue having been noted as a limiting factor in other simple dispersion cancellation methods, eg [13]. The applicability of the method is based on the fact that a random distribution of events in energy will give rise to indistinguishable time profiles (or CDFs) that can thus be directly compared using some kind of statistical metric, among which the *Kolmogorov metric* was found

by us to be best suited to our purposes. When used in conjunction with unbinned algorithms for identifying variability features like flares in lightcurves, such as for example the Bayesian Blocks algorithm[19], the analysis chain would be an entirely non-parametric way to search for energy dependent dispersion (though such an analysis is beyond the scope of this rather specific discussion).

We have discussed in detail the factors contributing to the uncertainty in the determination of a lag, and the method was subsequently applied to the challenging case study of looking for a small magnitude dispersion expected from a specific QG-induced LIV, following the form of equation 1. It is already known that there is no dispersion present in the PKS 2155-304 big flare night lightcurve that is any larger than the limits achievable by our method, presented in table 2 [1], therefore we did not attempt to derive further limits using that exemplary dataset. It should be noted, however, that the limits for each of the simulated sub-flares are at least a factor of two better than the cross-correlation method of [1] and comparable to the much more complex analysis of [2]; but while those two methods used the entire night's lightcurve as a single dataset to derive their limits this method has the advantage of being able to treat distinct bursts within the lightcurve as independent tests. Analysing a larger number of individual sub-flare features with the method presented here, and posteriorly combining a statistical sample of flares to obtain a single estimate (or limit) on dispersion could correspondingly make for yet more constraining limits on LIV.

In section 3.5 we found the intuitive result that the uncertainty in any measured dispersion scales inversely with the hardness of the energy spectrum. This also leads to the slightly counter-intuitive consequence that a nearer AGN such as Mrk 421 in a high state (eg [20, 21]) could provide as constraining a limit, if not more so, than a more distant object (like PKS 2155-304) if it showed similar variability timescales. This is solely due to the harder observed spectra, meaning an increased number of high energy photons being detectable from the nearer object (due to less absorption by the extragalactic background light). This could give a smaller uncertainty on the dispersion even if the expected magnitude of the delays are smaller. At a redshift of $z \sim 0.03$ for Mrk 421, the expected dispersion would be $\tau \sim 1 \text{ s/TeV}$ for Planck mass scale quantum gravity; with a next generation observatory such as CTA [22] the number of photons above 10 TeV in minute scale flares could potentially push the expected sensitivity η an order of magnitude beyond what is achievable today with AGN studies. This means that such AGN studies could perhaps surpass even the current Fermi limits on GRB 090510 [6] making for a useful independent confirmation of that result. The combined information from different source classes and over a sufficient range in redshift would then enable to distinguish between intrinsic source and external propagation induced dispersion effects.

The performance on the method has been tested on a specific case, but this method is, of course, not just limited to searches for a linear expansion term and VHE gamma-ray observations provide the highest energy photon datasets for probing the quadratic term of equation 1 (e.g., [2]). The simple isotropic dispersion scheme of equation 1 also neglects a number of aspects of potential Lorentz violation effects, such as birefringence and direction dependent vacuum co-efficients for Lorentz invariance (see eg equation 145 of [23]) which could make up interesting follow-up studies with either this or next generation gamma-ray telescope datasets. Neither is our method just limited to ground based VHE gamma-ray datasets, the extended baseline for the Fermi GRB datasets can more than compensate for the lower photon energies (with regard to the linear term, [6]), and tests for birefringency effects (which instead cause a spread in the wave packets [23]) have been made using INTEGRAL observations of the highly polarised GRB 041219A. Unfortunately it is not currently possible to determine the polarisation of gamma-rays from ground

based observations, so this case has not be dealt with here, but broadening of the lightcurve can also arise in certain models that predict a stochastic, super-luminal aspect to the refractive index (eg [24]), though such tests may be better aided with a metric that is optimal in testing the change in kurtosis of the lightcurve, rather than the skewness, as used here.

Most importantly of all, the method for testing for the presence of a dispersion is not limited to just testing for Lorentz invariance violation effects. Indeed any physical model that introduces a width or a delay in the emission, such as acceleration within the emission region (eg [25]) or due to cascading on the intergalactic magnetic field (eg [26]), can be adopted as the model for the time delay correction. These are all tests to be pursued in future work and not in the scope of this paper, which is to present the method, its benefits and limitations.

Acknowledgements

We thank P. M. Chadwick for useful comments on the original work. We also thank the anonymous referees for many critical comments which helped to improve very much this manuscript. UBdA acknowledges a PhD Scholarship from the CAPES Foundation, Ministry of Education of Brazil.

Appendix A. Light Curve Representation

In order to apply the algorithm, it is necessary to define how to construct the CDFs from the low and high-energy event sequences of the burst under study (step 3 of the analysis procedure). Given that the Kolmogorov distance is a metric for probability distributions, the event sequence must be normalised. Since the dataset is composed of time- and energy-tagged events, the cancellation will be applied to every photon individually so that none of the available information is left out of the analysis. The simplest choice for representing the data is therefore to construct empirical CDFs for both the low- and high-energy profiles as step functions from the original event sequence, according to the following rule:

$$CDF : F(t_i) = i/N, \quad (\text{A.1})$$

where t_i is the time of the i^{th} event in the sequence, and N is the total number of events in the sequence. In this construction, the height of each step is constant and equal to N^{-1} (the CDF is defined between 0 and 1), and the length of each step equals the waiting time between events in the sequence. All the timing information of the temporal sequence is thus explicitly preserved in this representation.

A different representation of the dataset was proposed in Scargle et al. (2008) [13], and can be used as an alternative way of constructing the CDF. In this representation, the dataset is tessellated so that the photon sequence is represented by a series of cells of width dt_i constructed around each event i . A cell density is then defined by the rule $x_i = 1/dt_i$, which can be interpreted as the instantaneous rate of the process at time t_i , which is later normalised into a discrete probability distribution: $p_i = x_i / \sum x_i$. The CDF in this case would be:

$$CDF : F(t_i) = \sum_{l < t_i} p_l, \quad (\text{A.2})$$

For the application of the Kolmogorov distance metric, we found that the first representation in equation A.1 is more appropriate. This is because the magnitude of the cell densities representation can be dominated by spikes resulting from very small inter-event times in some cells,

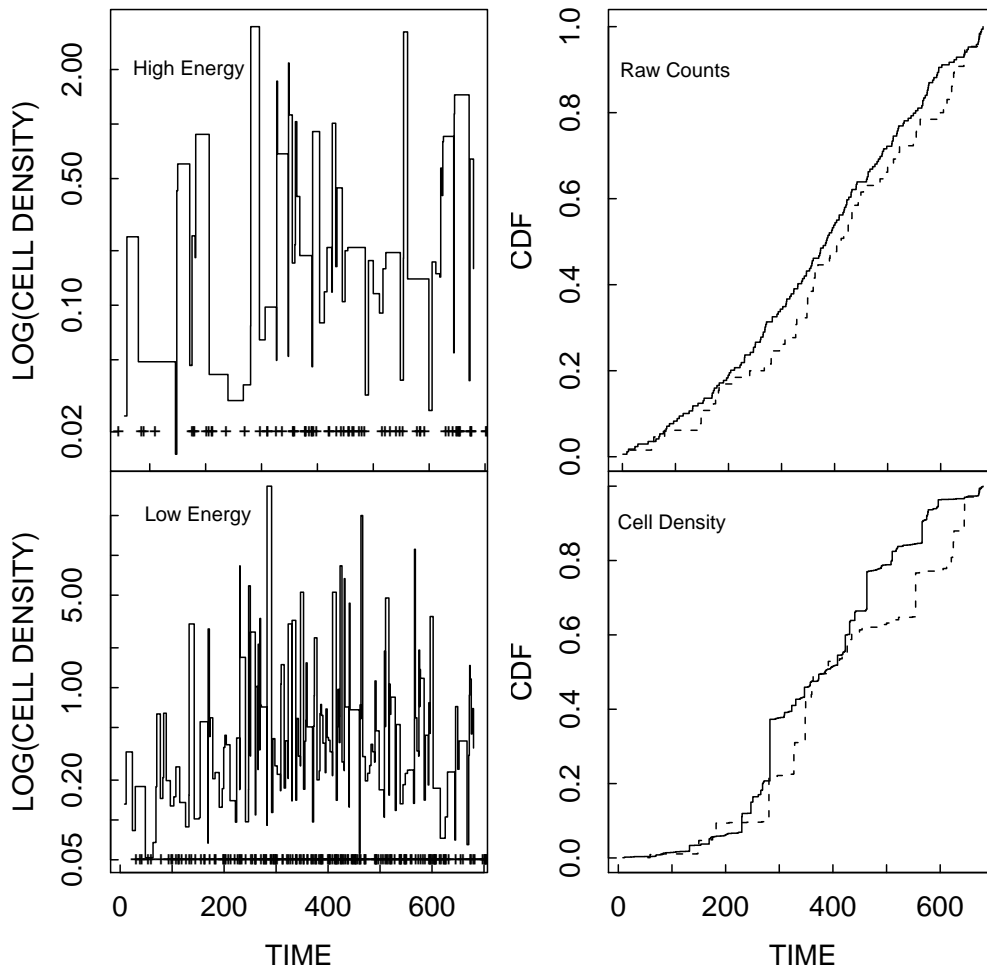


Figure A.12: Choice of the light-curve representation. The panels on the left show the cell density representation for the low- and high-energy components of flare BF1 of PKS 2155-304 (see 4 for nomenclature of the flares). The right panels show the correspondent CDFs for the two light-curve representations discussed. Note that the *raw events* representation shows considerably less “raggedness” in the CDFs than the *cell density* one, and is therefore more appropriate for calculating the Kolmogorov distance cost-function.

originating from the noise of the Poisson process, which will introduce excessive “raggedness” in the CDF representation. This can be seen in the right panel of figure A.12 where we compare the low- and high-energy CDFs from a simulated burst profile based on the burst BF1 of the VHE flare of PKS 2155-304 observed with H.E.S.S. In this case, both profiles superpose, as there is no significant dispersion present, but the cell density representation results in additional fluctuations in the constructed CDFs. A way to circumvent this problem within the cell representation is to adopt a logarithmic scale for the density – for example $x_i = \log(1/dt_i)$ – which better recovers the shape of the profile.

- [1] Hess Collaboration, F. Aharonian, et al, Limits on an Energy Dependence of the Speed of Light from a Flare of the Active Galaxy PKS 2155-304, *Physical Review Letters* 101 (17) (2008) 170402–+. [arXiv:0810.3475](#), [doi:10.1103/PhysRevLett.101.170402](#).
- [2] Hess Collaboration, A. Abramowski, et al, Search for Lorentz Invariance breaking with a likelihood fit of the PKS 2155-304 flare data taken on MJD 53944, *Astroparticle Physics* 34 (2011) 738–747. [arXiv:1101.3650](#), [doi:10.1016/j.astropartphys.2011.01.007](#).
- [3] S. Sarkar, Possible Astrophysical Probes of Quantum Gravity, *Modern Physics Letters A* 17 (2002) 1025–1035. [arXiv:arXiv:gr-qc/0204092](#), [doi:10.1142/S0217732302007521](#).
- [4] G. Amelino-Camelia, J. Ellis, N. E. Mavromatos, D. V. Nanopoulos, S. Sarkar, Tests of quantum gravity from observations of γ -ray bursts, *Nature* 395 (1998) 525–+. [doi:10.1038/26793](#).
- [5] MAGIC Collaboration, J. Albert, et al, Probing quantum gravity using photons from a flare of the active galactic nucleus Markarian 501 observed by the MAGIC telescope, *Physics Letters B* 668 (2008) 253–257. [arXiv:0708.2889](#), [doi:10.1016/j.physletb.2008.08.053](#).
- [6] Fermi-LAT Collaboration A. A. Abdo, et al., A limit on the variation of the speed of light arising from quantum gravity effects, *Nature* 462 (2009) 331–334. [arXiv:0908.1832](#), [doi:10.1038/nature08574](#).
- [7] Hess Collaboration, F. Aharonian, et al, An Exceptional Very High Energy Gamma-Ray Flare of PKS 2155-304, *Astrophysical Journal Letters* 664 (2007) L71–L74. [arXiv:0706.0797](#), [doi:10.1086/520635](#).
- [8] Fermi-LAT Collaboration A. A. Abdo, et al., Fermi Observations of High-Energy Gamma-Ray Emission from GRB 080916C, *Science* 323 (2009) 1688–. [doi:10.1126/science.1169101](#).
- [9] E. Troja, S. Rosswog, N. Gehrels, Precursors of Short Gamma-ray Bursts, *ApJ* 723 (2010) 1711–1717. [arXiv:1009.1385](#), [doi:10.1088/0004-637X/723/2/1711](#).
- [10] Fermi-LAT Collaboration W. B. Atwood, et al., The Large Area Telescope on the Fermi Gamma-Ray Space Telescope Mission, *ApJ* 697 (2009) 1071–1102. [arXiv:0902.1089](#), [doi:10.1088/0004-637X/697/2/1071](#).
- [11] M. Martínez, M. Errando, A new approach to study energy-dependent arrival delays on photons from astrophysical sources, *Astroparticle Physics* 31 (2009) 226–232. [arXiv:0803.2120](#), [doi:10.1016/j.astropartphys.2009.01.005](#).
- [12] T. Li, J. Qu, H. Feng, L. Song, G. Ding, L. Chen, Timescale Analysis of Spectral Lags, *Chinese Journal of Astronomy and Astrophysics* 4 (2004) 583–598. [arXiv:arXiv:astro-ph/0407458](#).
- [13] J. D. Scargle, J. P. Norris, J. T. Bonnell, An Algorithm for Detecting Quantum Gravity Photon Dispersion in Gamma-Ray Bursts: DisCan, *ApJ* 673 (2008) 972–980. [doi:10.1086/524396](#).
- [14] J. Ellis, N. Harries, A. Mereghaglia, A. Rubbia, A. S. Sakharov, Probes of Lorentz violation in neutrino propagation, *Physical Review D* 78 (3) (2008) 033013–+. [arXiv:0805.0253](#), [doi:10.1103/PhysRevD.78.033013](#).
- [15] A. Kolmogorov, General measure theory and probability calculus, *Selected Works of Andrei Kolmogorov - Probability Theory and Mathematical Statistics* 2 (1992) 48–59.
- [16] W. H. Press, S. A. Teukolsky, W. T. Vetterling, B. P. Flannery, *Numerical recipes in FORTRAN. The art of scientific computing*, 1992.
- [17] J. P. Norris, R. J. Nemiroff, J. T. Bonnell, J. D. Scargle, C. Kouveliotou, W. S. Paciesas, C. A. Meegan, G. J. Fishman, Attributes of Pulses in Long Bright Gamma-Ray Bursts, *ApJ* 459 (1996) 393–+. [doi:10.1086/176902](#).
- [18] VERITAS Collaboration D. B. Kieda et al, Orbit Mode observations of Crab and Mrk 421, *ArXiv e-prints* [arXiv:1110.5974](#).
- [19] J. D. Scargle, *Studies in Astronomical Time Series Analysis. V. Bayesian Blocks, a New Method to Analyze Structure in Photon Counting Data*, *ApJ* 504 (1998) 405–+. [doi:10.1086/306064](#).
- [20] M. Błażewski, et al, A Multiwavelength View of the TeV Blazar Markarian 421: Correlated Variability, Flaring, and Spectral Evolution, *ApJ* 630 (2005) 130–141. [arXiv:arXiv:astro-ph/0505325](#), [doi:10.1086/431925](#).
- [21] VERITAS Collaboration V. A. Acciari, et al, TeV and Multi-wavelength Observations of Mrk 421 in 2006-2008, *ArXiv e-prints* [arXiv:1106.1210](#).
- [22] M. Actis, G. Agnetta, F. Aharonian, A. Akhperjanian, J. Aleksić, E. Aliu, D. Allan, I. Allekotte, F. Antico, L. A. Antonelli, P. Antoranz, A. Aravantinos, T. Arlen, H. Araldi, S. Artmann, K. Asano, H. Asorey,

- J. Bähr, A. Bais, C. Baixeras, et al., Design concepts for the Cherenkov Telescope Array CTA: an advanced facility for ground-based high-energy gamma-ray astronomy, *Experimental Astronomy* 32 (2011) 193–316. doi:10.1007/s10686-011-9247-0.
- [23] V. A. Kostelecký, M. Mewes, Electrodynamics with Lorentz-violating operators of arbitrary dimension, *Phys. Rev. D* 80 (1) (2009) 015020. arXiv:0905.0031, doi:10.1103/PhysRevD.80.015020.
- [24] N. E. Mavromatos, String Quantum Gravity, Lorentz-Invariance Violation and Gamma Ray Astronomy, *International Journal of Modern Physics A* 25 (2010) 5409–5485. arXiv:1010.5354, doi:10.1142/S0217751X10050792.
- [25] W. Bednarek, R. M. Wagner, A model for delayed emission in a very-high energy gamma-ray flare in Markarian 501, *A&A* 486 (2008) 679–682. arXiv:0804.0619, doi:10.1051/0004-6361:20079068.
- [26] A. Neronov, D. V. Semikoz, Sensitivity of γ -ray telescopes for detection of magnetic fields in the intergalactic medium, *Phys. Rev. D* 80 (12) (2009) 123012. arXiv:0910.1920, doi:10.1103/PhysRevD.80.123012.